Visual Comput (2006) 22: 43–55
DOI 10.1007/s00371-005-0352-9

ORIGINAL ARTICLE

Liyan Zhang
Anshuman Razdan
Gerald Farin
John Femiani
Myungsoo Bae
Charles Lockwood

3D face authentication and recognition based on bilateral symmetry analysis

Published online: 21 October 2005

L. Zhang (✉)
Nanjing University of Aeronautics and Astronautics, Nanjing, 210016, P.R. China
zhangly@nuaa.edu.cn

A. Razdan · G. Farin · J. Femiani · M. Bae
PRISM, Arizona State University, Tempe, AZ85287, USA
{razdan, gerald.farin, john.femiani, myungsoo.bae}@asu.edu

C. Lockwood
Department of Anthropology, University College London, London WC1E 6BT, UK
c.lockwood@ucl.ac.uk

Abstract We present a novel and computationally fast method for automatic human face authentication. Taking a 3D triangular facial mesh as input, the approach first automatically extracts the bilateral symmetry plane of the facial surface. The intersection between the symmetry plane and the facial surface, namely the symmetry profile, is then computed. Using both the mean curvature plot of the facial surface and the curvature plot of the symmetry profile curve, three essential points of the nose on the symmetry profile are automatically extracted. The three essential points uniquely determine a Face Intrinsic Coordinate System (FICS). Different faces are aligned based on the FICS. The symmetry profile, together with two transverse profiles, composes a compact representation, called the SFC representation, of a 3D face surface. The face authentication and recognition steps are finally performed by comparing the SFC representations of the faces. The proposed method was tested on 382 face surfaces, which come from 166 individuals and cover a wide ethnic and age variety. The equal error rate (EER) of face authentication on scans with variable facial expressions is 10.8%. For scans with normal expression, the ERR is 0.8%.

Keywords Face authentication · Face recognition · Symmetry analysis · 3D faces

1 Introduction

Automatic face authentication has long been an active research area because of its potential for applications such as law enforcement, security access, and man–machine interaction. Most of the extensive recognition literature concerns 2D methods (see [23] for an overview). Among various approaches, principal component analysis (PCA) [20], or the eigenface method, is now a cornerstone in face recognition. However, 2D face recognition methods are in general unable to overcome the problems resulting from illumination, expression, or pose variations. An emerging trend in the field of face recognition is 3D technology, which is expected to be more accurate and able to overcome the problems of 2D methods, as true 3D information is independent of viewpoint and lighting conditions.

There are several strategies in 3D face recognition: segmentation of the face surface into meaningful points, lines, and regions [11, 17]; model-based approaches using information about texture, edge form, and color [5, 14]; various PCA-based methods [7, 9]; facial indexing by point signatures [10]; and multiple-profile comparisons [3, 8, 22]. A comprehensive survey on 3D face recognition can be found in [6].

The highest rates of correct recognition on large samples have been achieved by Chang et al. [9]. They used both 2D and 3D face information for the recognition task. In their experiments, a PCA-based approach was tuned for face recognition from 2D intensity images and 3D range images. When methods were analyzed separately,

3D outperformed 2D information. By combining the 2D distance measure and the 3D distance measure, a 2D-plus-3D criterion was used during the decision process of face recognition. In their experiments, pose variations that occur during the acquisition process were manually normalized. The recognition rate of the combination scheme was reported to be higher than 98% under the condition that the 2D and 3D images were taken in a front view and the subjects imaged with a normal facial expression. The same research group reported later that recognition rates fell to 55% when variations were allowed in facial expression [6]. For that reason methods are still being sought that focus on rigid parts of the face.

The background most relevant to our 3D approach has to do with profile comparisons. In particular, Beumier et al. [3] developed an integrated 3D face acquisition and comparison system based on multiple-profile comparisons. Structured light was used to capture the facial surface. For facial surface comparison, they calculated the global matching error of the facial surfaces. An iterative condition mode (ICM) optimization was performed to determine the rotation and translation transform that minimizes the global matching error sampled at 15 profiles. In order to speed up the global matching process, they further extracted the central profile with maximal protrusion (due to the nose). The central profile and a mean lateral profile were used to compare two faces in the curvature space. The main advantages of this method are its high speed and low storage needs. But as the authors pointed out, the optimization procedure used for the 3D face comparison can fail due to bad initial parameters. To improve the EER (equal error rates, see Sect. 5.2 for details), they resorted to manual refinement for surface matching. In [4], Beumier et al. further explored a geometry plus gray level scheme, which improves the recognition rate. Cartoux et al. [8] presented a similar approach to extract the symmetry profile by looking for the bilateral symmetry axis of Gaussian curvature values of the facial surface. Their method was tested on five people; thus applicability of this method on a large test database remains untested. Wu et al. [22] use the central profile and two transverse profiles for face authentication. In their symmetry analysis, an initial position of the symmetry plane needs to be interactively set. The number of individuals in the database used in [3] and [22] is 30.

In this paper, we explore the applicability of the profile-based scheme in a larger-scale database, which covers a wide ethnicity, expression, and age variety. Our work is based on the assumption that the human face is bilaterally symmetric, and this property is the key to developing fast, accurate algorithms of recognition. We fully automate the extraction of a symmetry plane, without any prior knowledge about the coordinate systems of the scanners and the head pose. A novel method based on both the mean curvature plot of the facial surface and the curvature plot of the symmetry profile curve is used to accurately extract three essential points of the nose on the symmetry profile. The three essential points uniquely determine a Face Intrinsic Coordinate System (FICS), which is used to align different faces for comparison. The symmetry profile, together with two transverse profiles, namely the forehead profile and the cheek profile, compose a compact representation, called the SFC representation, of a 3D facial surface. The face authentication and recognition steps are finally performed by comparing the SFC representation of the faces.

The 3D surface here is a triangular mesh, which is the most popular representation of 3D geometry. Many types of scanners can output triangular meshes directly or by means of surface reconstruction software. Thus our method is applicable to data obtained by different scanners used at different locations.

The rest of this paper is organized as follows. Section 2 describes the symmetry plane extraction method. In Sect. 3, an algorithm for extracting the three essential points on the symmetry profile is presented. Section 4 gives the similarity measures based on a profile comparison. Section 5 introduces and analyzes the experimental results of the proposed approach. Finally, Sect. 6 concludes the paper and points out future work.

2 Symmetry plane extraction

A 3D object is bilaterally symmetric if there exists some plane such that the object is invariant under reflection about that plane. Bilateral symmetry computation of shapes and images is a basic problem in the fields of mathematics, computer vision, and image processing. Most symmetry extraction algorithms are designed for 2D applications (e.g., [15] and [19]), but a variety of methods have recently been developed for 3D applications [1, 13, 16, 18, 21, 22].

Following [1, 22] and others, we use a mirror transformation followed by a registration procedure to extract the symmetry plane of a human face. To make the entire process automatic and pose-invariant, we first determine the most appropriate position of the mirror plane by means of principal component analysis (PCA), so that the original mesh and the mirrored mesh are approximately aligned. The iterative closest point (ICP) algorithm is then used to get a refined registration [2].

2.1 Mirror plane determination

Let $S(P, K)$ denote the triangular facial mesh surface, where P is a set of N point positions $\boldsymbol{p}^i(x^i, y^i, z^i) \in R^3$, $1 \le i \le N$ and K is an abstract simplicial complex that contains the adjacency information of $vertices : v = \{i\} \in K$, $edges : e = \{i, j\} \in K$ and $triangles : f = \{i, j, k\} \in K$.

Suppose the column vector $\boldsymbol{O}_s$ is the centroid of the facial mesh $S(P, K)$. We first construct the covariance ma-

trix of the vertex distribution as follows:

$$C = \sum_{i=0}^{N} (\boldsymbol{p}^i - \boldsymbol{O}_s)(\boldsymbol{p}^i - \boldsymbol{O}_s)^T . \quad (1)$$

By means of PCA we can get three eigenvalues $\lambda_1 \geq \lambda_2 \geq \lambda_3$ and the three corresponding eigenvectors $\boldsymbol{v}_1$, $\boldsymbol{v}_2$, $\boldsymbol{v}_3$ of C. The facial surface is typically taller than it is wide, i.e., the vertical dimension is longer than the horizontal dimension. Thus, the covariance matrix C is expected to have three different eigenvalues. The eigenvector $\boldsymbol{v}_3$ represents the normal direction of the least squares fitted plane of the facial surface. The eigenvector $\boldsymbol{v}_1$ corresponds to the vertical dimension of the facial surface. The complexity of the PCA algorithm is $O(N)$.

Taking $\boldsymbol{O}_s$ as the origin, $\boldsymbol{v}_1$ as the y axis, and $\boldsymbol{v}_3$ as the z axis, we define a new right-hand coordinate system. This coordinate system is called the pose coordinate system (PCS), for it represents the head pose and depends only on the vertex distribution of the facial surface. The original facial surface $S(P, K)$ is first transformed to the PCS. We then use the yz-coordinate plane of the PCS as the mirror plane to get a mirrored facial surface S_m. This procedure can be described as

$$\begin{aligned} &\boldsymbol{p}_m^i \leftarrow R \cdot A \cdot (\boldsymbol{p}^i - \boldsymbol{O}_s) , \\ &\boldsymbol{p}^i \leftarrow A \cdot (\boldsymbol{p}^i - \boldsymbol{O}_s) , \\ &R = \begin{bmatrix} -1 & 0 & 0 \\ 0 & 1 & 0 \\ 0 & 0 & 1 \end{bmatrix}, \quad A = \begin{bmatrix} v_2^x & v_1^x & v_3^x \\ v_2^y & v_1^y & v_3^y \\ v_2^z & v_1^z & v_3^z \end{bmatrix} , \end{aligned} \quad (2)$$

where $\boldsymbol{p}_m^i$ is the mirrored point of $\boldsymbol{p}^i$, A is the rotation matrix from the original coordinate system to the PCS, R is the reflection matrix with respect to the mirror plane, v in matrix A represents the components of the eigenvectors $\boldsymbol{v}_1$, $\boldsymbol{v}_2$, and $\boldsymbol{v}_3$ of C.

The first row of Fig. 1 shows the results of the intersection between the estimated mirror plane and the facial mesh surface on four individuals. It is known that if a physical object is bilaterally symmetric, then the symmetry plane passes through its centroid and is orthogonal to some principal axis. Figure 1 demonstrates that the mirror plane computed using PCA is close to the symmetry plane but not accurate in some cases. This is because (1) the face itself is not perfectly symmetric; (2) the centroid $\boldsymbol{O}_s$ is obtained by averaging all the vertices in the facial mesh S, but the distribution of the vertices of the meshes is generally not even; and (3) the boundary of the mesh is irregular and may be strongly asymmetric.

2.2 Model registration

Since the mirror plane does not coincide with the real symmetry plane in most cases, there exists some misalignment between the mirrored mesh S_m and the original mesh S. We use the basic idea of the ICP algorithm [2] to get an optimized registration.

The ICP algorithm is the most popular method to register two 3D shapes. Given two 3D point sets C_1 and C_2, the main steps of the ICP algorithm are:

(1) For every point in C_2, compute its closest point in C_1.
(2) The mean square distance of the pairs of closest points is minimized with respect to a rigid body transform.

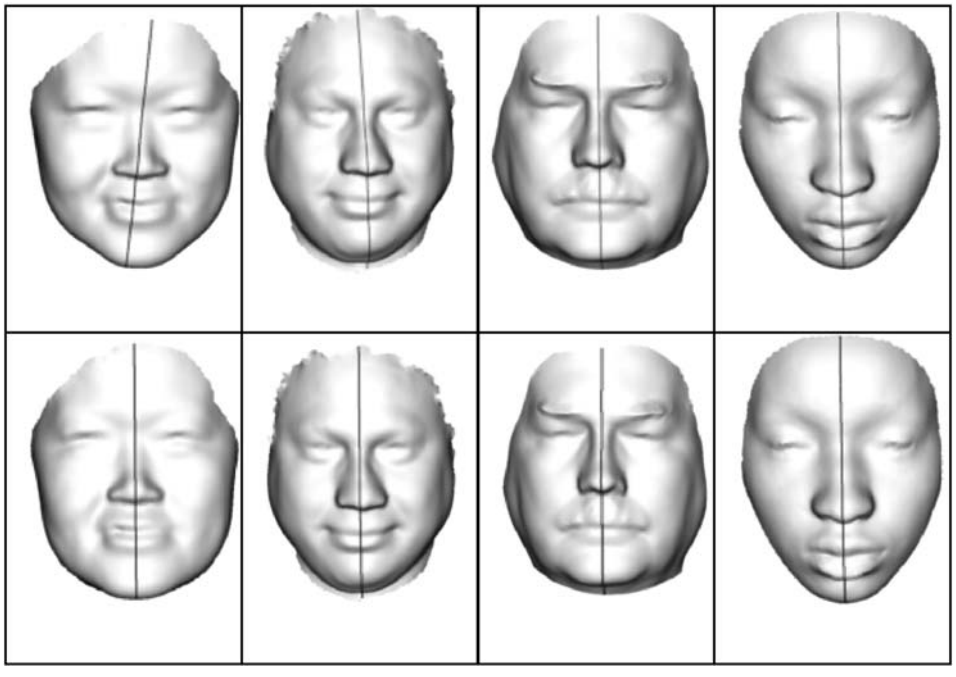

Fig. 1. Results of estimated mirror plane and extracted symmetry plane. *Black lines* in *first row*: intersection between mirror planes (by PCA algorithm) and facial meshes. *Second row*: intersection between automatically extracted symmetry planes and facial meshes (by aligning mirrored and original facial meshes; see Sects. 2.2 and 2.3)

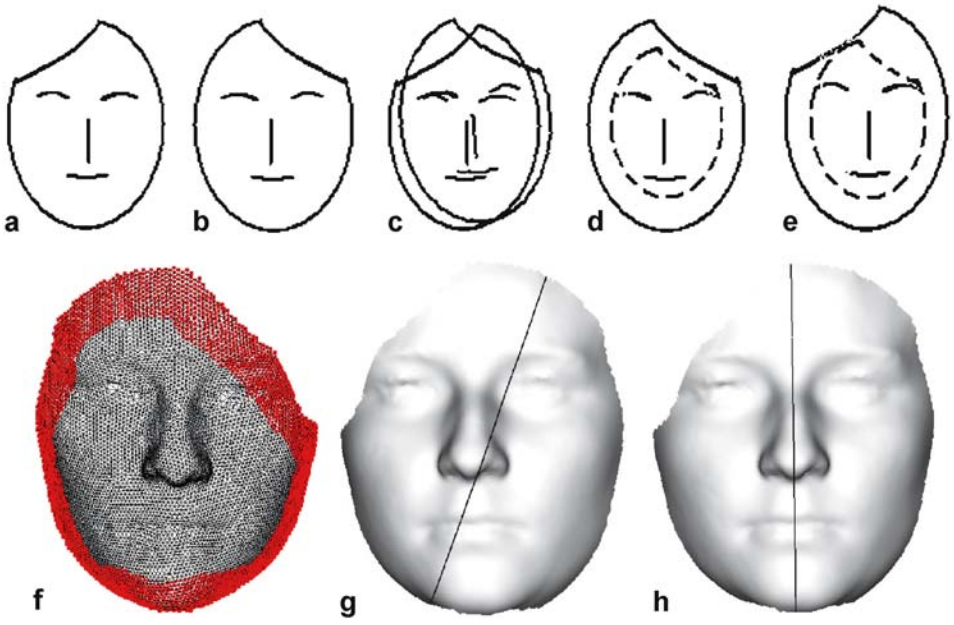

Fig. 2a–h. Illustration for MarkSkirt operator. **a** 3D facial mesh with incomplete boundary. **b** Mirrored mesh. **c** Alignment of **a** and **b** using ICP algorithm directly, which is not expected. The region between the boundary and the *dashed curve* on the mirrored mesh in **d** is called the Skirt. **e** Alignment of nonskirt region on S_m and original mesh S, which represents expected correct alignment. **f–h** Example where part of forehead is missing due to occlusion of hair. *Red* vertices in **f** are $Skirt(S_m)$. **g** Computed symmetry plane without MarkSkirt operator. **h** Result with MarkSkirt operator

(3) Apply the transform to C_2.
(4) Terminate the iteration if the change in mean square distance falls below a preset threshold; otherwise, return to step (1).

In our case, the two datasets are vertices of the facial meshes S and S_m. Since the boundary of the facial mesh could be irregular (Fig. 2a), directly using the ICP algorithm may make S and S_m misaligned (Fig. 2c), which leads to an incorrect symmetry plane. To solve this problem, we employ an operator called MarkSkirt. First, we introduce the neighborhood relation *nbhd* in the mesh surface $S(P, K)$:

$$nbhd\{i\} := \{i\} \cup \{j | \exists \{i, j\} \in K\} ,$$
$$nbhd\{i_1, i_2, \ldots, i_k\} := \cup_{\mu=1,\ldots,k} nbhd\{i_\mu\} . \quad (3)$$

We also use the following recursive definition:

$$nbhd^1\{i\} := nbhd\{i\} ,$$
$$nbhd^n\{i\} := nbhd\{nbhd^{n-1}\{i\}\} \qquad n \geq 2 . \quad (4)$$

$nbhd^n\{i\}$ is also called the n-ring neighbors of vertex $\{i\}$. The MarkSkirt operator finds and marks the n-ring neighbors of all the vertices on the boundary of the mirrored mesh S_m as Skirt. This is defined as

$$Skirt(S_m) := \{j | j \in \cup_{\{i\} \in \partial S_m} nbhd^n\{i\}\} , \quad (5)$$

where ∂S_m represents the boundary of S_m.

After the MarkSkirt procedure, we obtain:

$$P'_m = P_m \backslash Skirt(S_m) , \quad (6)$$

where P_m denotes the vertex set of S_m. Only the vertices in P'_m are sampled to match with the original mesh S. This is to make sure that the region to be matched with the original mesh S is the subset of S (Fig. 2e), for the ICP algorithm performs well in this situation. In our experiments, 10-ring neighbors of the boundary are marked as Skirt. The MarkSkirt operator is crucial to get a correct alignment when the facial mesh boundary is irregular and asymmetric. Figure 2f–h illustrates the effect of the MarkSkirt operator. Our experiments show that about 15% of faces give unexpected alignment without the MarkSkirt operator. With this operator, however, all of the 382 faces provide visually pleasing symmetry planes (even though some of the tested faces have asymmetric expressions). When an individual face is slightly asymmetric, its intrinsic asymmetry will be reproduced in different scans, and hence will not affect decision making in authentication and recognition tasks.

The complexity in Steps (2) and (3) of the ICP algorithm are $O(N)$. But in Step (1), the complexity for computing the entire set of the closest points is $O(N^2)$, and the computation needs to be performed in every iteration. The ICP algorithm is normally time consuming, due to the cost of finding the closest points. In our application, two methods are used to speed up the ICP algorithm. First,

partial (randomly sampled) instead of entire vertices of P'_m are used to match with the original mesh S. In the implementation, 300 randomly selected vertices (about 5% of the all the vertices in P'_m of the facial meshes in our experiments) are used. This is reasonable because of the fact that the ICP algorithm performs well when one dataset is the subset of the other one. We further speed up the closest points finding process by using a space partitioning scheme. In Sect. 2.1, we have transformed the facial mesh S to the PCS. Now we construct in PCS an axis-aligned bounding box that encloses both S and S_m. The bounding box is then partitioned into $m \times n \times l$ cells. The searching for the closest vertex $\{i\} \in S_m$ can be limited to the cells surrounding $\{i\}$. In our experiments, the number of cells m in the x direction (corresponding to the approximate left/right direction) is set to 10. Suppose the edge lengths of the bounding box in the x, y, and z directions are l_x, l_y, and l_z, respectively, then $n = 10 * l_y/l_x$, and $l = 10 * l_z/l_x$.

Our experiments show that the above-mentioned schemes for accelerating the algorithm are effective. The average time spent on the process of ICP is 1.2 s (see Sect. 5.4 for more information on computation time). A good initial relative position of S and S_m, due to the adequate mirror plane computed by the PCA, not only gives more chances to achieve the globally optimized registration but also contributes to the rapid convergence of the ICP algorithm. Table 1 illustrates the mean distance between the pairs of closest points of the original mesh and the mirrored one for four individuals in Fig. 1. From the values in the table we can see that the ICP procedure improves the alignment to various extents for different individuals. We also find that if the boundary of the facial mesh is good enough (e.g., that of person 4 in Fig. 1), the PCA algorithm itself can generate a good mirror plane that is very close to the bilateral symmetry plane of the face.

Table 1. Mean distance between original mesh and mirrored one, before and after ICP algorithm

Mean Dis. (mm)	Person 1	Person 2	Person 3	Person 4
Before ICP	3.088	2.329	1.162	1.162
After ICP	1.316	1.103	1.030	0.958

2.3 Symmetry profile extraction

After the original facial surface S and the mirrored surface S_m have been registered, the symmetry plane can be easily fitted. Define

$$\boldsymbol{p}_c^i = \tfrac{1}{2}(R_{ICP} \cdot (\boldsymbol{p}_m^i - \boldsymbol{t}_{ICP}) + \boldsymbol{p}^i) \quad , \quad i = 1, 2, \ldots N \, , \tag{7}$$

where R_{ICP} and $\boldsymbol{t}_{ICP}$ are, respectively, the rotation matrix and the translation vector output by the ICP algorithm. The midpoints $\boldsymbol{p}_c^i$, $i = 1, 2, \ldots, N$ are used to fit a least squares plane, which is the final symmetry plane, denoted PL^s. The symmetry profile of a face is extracted by intersecting PL^s with the facial surface S. The complexity of this process is $O(\sqrt{N})$.

The second row in Fig. 1 shows the final symmetry planes of the four individuals.

3 Symmetry profile analysis

The symmetry profile extraction provides a basic method of face authentication. However, the vertical orientation of the profile (forehead vs. chin) is unknown, since we do not assume any prior knowledge about the coordinate systems of the scanners and the head pose. The next step, therefore, is to automatically determine essential points on the symmetry profile and, in so doing, orient the profile correctly.

The symmetry profile passes through several distinctive facial features: the forehead, the bridge of the nose, the nose itself, the philtrum, the mouth, and the chin. Of these, the nose is the most robust geometrical feature on the symmetry profile (and on the entire face). It is least changed under different expressions and contains clearly distinguishable points. Profile curvature itself does not reliably identify the nose: the point corresponding to the largest curvature might be the nose tip, the upper or lower mouth lip, the conjunction point between the nose and the philtrum, or other landmarks. Because of this, we identify the nose from a combination of overall facial surface curvature analysis and symmetry profile curvature analysis.

3.1 Mean curvature plot of facial surface

We first roughly isolate the nose from its surrounding area by means of facial surface curvature analysis. The principal curvature plot, the Gaussian curvature plot, the mean curvature plot, and the HK segment method were tested. The experiments show that the mean curvature plot is the most effective one to identify the nose.

We calculate the mean curvature on the facial mesh S by locally fitting a paraboloid, which is similar to the method presented in [12]. The difference is that we calculate the mean curvature value of the facial surface at the centroid of each triangle in the facial mesh, whereas the method in [12] calculates the curvature value at each vertex in the mesh surface. Taking the centroid of each triangle $\{i, j, k\}$ in S as the origin, we establish a paraboloid

$$\boldsymbol{Q}(u, v) = (u, v, h(u, v)) \, , \tag{8}$$

where

$$h(u, v) = au^2 + buv + cv^2 \, . \tag{9}$$

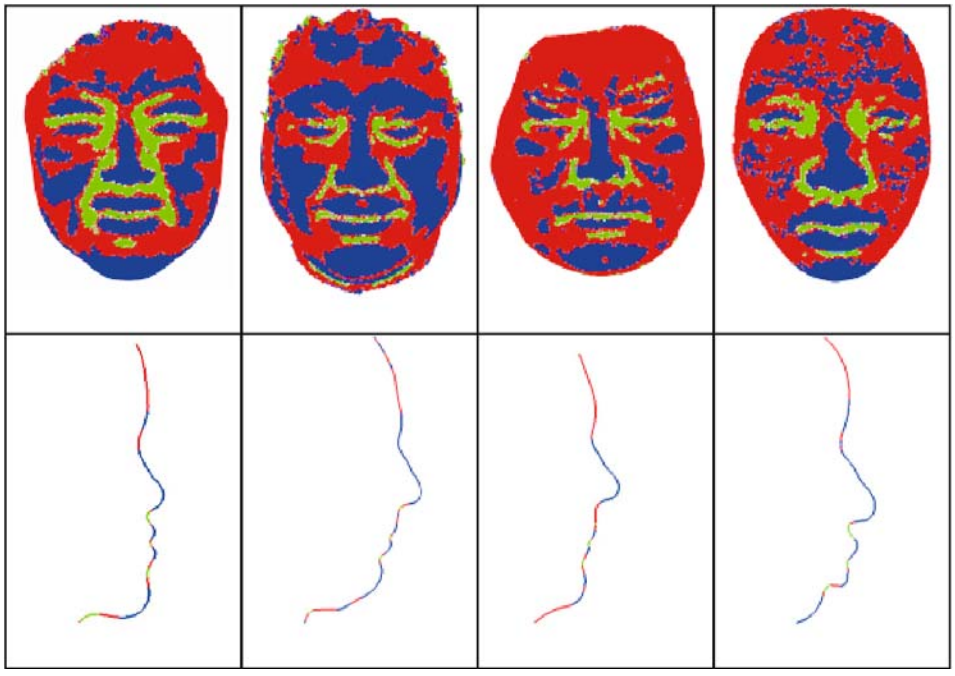

Fig. 3. Mean curvature plots of facial surfaces and colored symmetry profiles (Sect. 3.3)

The axis of h points to the normal direction of that triangle; u and v are in the triangle plane and orthogonal to each other. By substituting the one-ring neighbors of $\{i\}$, $\{j\}$, $\{k\}$ to the quadratic surface $\boldsymbol{Q}(u, v)$, the parameters a, b, and c can be determined by using least squares fitting. The curvature at $\boldsymbol{Q}(0, 0)$ is taken as the curvature at the centroid of triangle $\{i, j, k\}$. According to differential geometry, the mean curvature at $\boldsymbol{Q}(0, 0)$ is

$$H = a + c\,. \tag{10}$$

We classified the curvature values into three scales. Define

$$\begin{cases} H_1 = H_{\min} + \frac{1}{3}(H_{\max} - H_{\min})\,, \\ H_2 = H_{\min} + \frac{2}{3}(H_{\max} - H_{\min})\,, \end{cases} \tag{11}$$

where $H_{\max}$ and $H_{\min}$ are, respectively, the maximum and minimum mean curvature values. To eliminate the effect of noise, the 1% highest and lowest mean curvature values are not taken into account in searching for $H_{\max}$ and $H_{\max}$.

For triangle T_i, a color attribute is attached to it by

$$color(T_i) = \begin{cases} \text{“}blue\text{”} & if\ \ H_i < H_1\,, \\ \text{“}red\text{”} & if\ \ H_1 \le H_i \le H_2\,, \\ \text{“}green\text{”} & if\ \ H_i > H_2\,, \end{cases} \tag{12}$$

where H_i is the mean curvature value at the centroid of T_i.

The mean curvature plots in terms of the color attribute of four faces that have different noise levels are shown in the first row of Fig. 3. Our experiments on the 382 tested facial meshes show that the noses in the mean curvature plots are always blue, despite the large appearance variation among individuals. The mean curvature plot is used in Sect. 3.3 to extract some essential points on the symmetry profile.

3.2 Curvature analysis of symmetry profile

For analyzing the symmetry profile, we also need to calculate the curvature of the symmetry profile curve. Since the symmetry profile is generated by intersecting the symmetry plane with the facial mesh S, it is represented by a planar polyline. The curvature at each vertex $\boldsymbol{x}_i$ on the polyline is calculated by locally fitting a least squares parabola

$$\boldsymbol{q}(t) = (t,\, f(t))\,, \tag{13}$$

where

$$f(t) = a_c t^2 + b_c t + c_c\,. \tag{14}$$

Axes f and t are, respectively, the binormal and the tangent direction of the symmetry profile curve at $\boldsymbol{x}_i$. The curvature at $\boldsymbol{x}_i$, i.e., $\boldsymbol{q}(0)$, is

$$\kappa = 2a_c/(1 + b_c^2)^{\frac{3}{2}}\,. \tag{15}$$

Figure 4 illustrates the curvature plots of the symmetry profiles. From column 3 in Fig. 4 we can clearly see the curvature distribution along the symmetry profile. We can also see that the signs of the curvature at specific points, e.g., at the nose tips, are different in the two examples in Fig. 4. This is because one profile is from the forehead to the chin and the other is from the chin to the forehead.

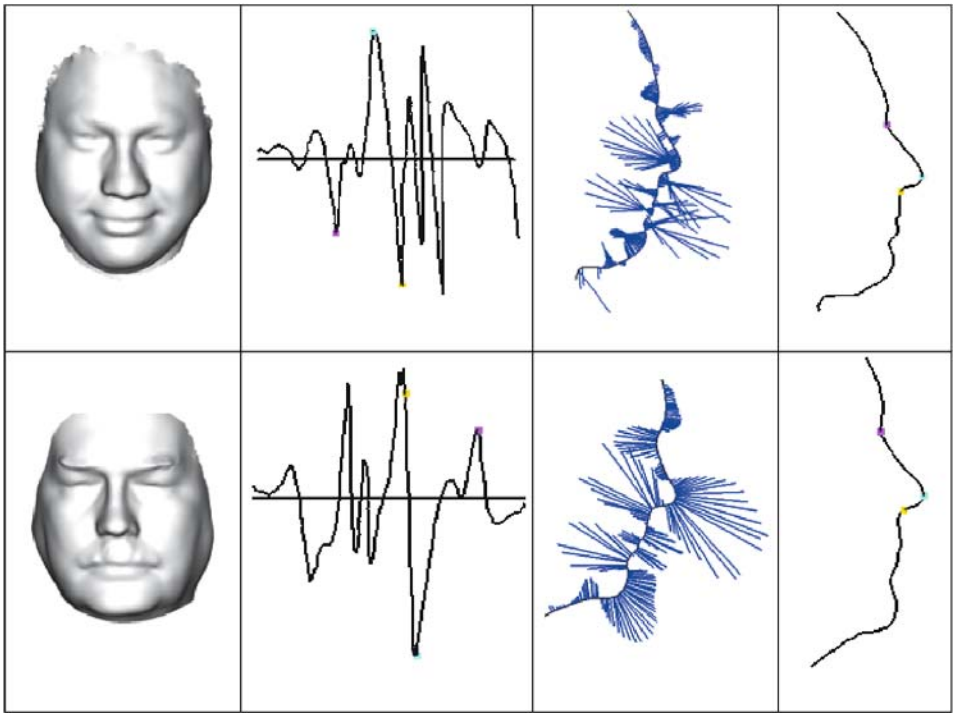

Fig. 4. Curvature plots and three essential points of symmetry profiles. The two *rows* illustrate the experimental results for two individuals. *Column 2*: curvature distribution with respect to arc length. *Column 3* is generated by attaching a line segment along normal direction at each point of symmetry profiles. Length of segment is proportional to signed curvature at that point. The *light blue, purple*, and *yellow points* are the automatically extracted three essential points $\boldsymbol{P}_{\mathrm{NT}}$, $\boldsymbol{P}_{\mathrm{NB}}$, and $\boldsymbol{P}_{\mathrm{NL}}$, respectively (Sect. 3.3)

3.3 Recognition of essential points

In this section, we use the mean curvature of the facial surface and the curvature of the symmetry profile to recognize three essential points on the symmetry profile, namely the nose tip (denoted as $\boldsymbol{P}_{\mathrm{NT}}$), the nose bridge (denoted as $\boldsymbol{P}_{\mathrm{NB}}$), and the lowest point of the nose (denoted as $\boldsymbol{P}_{\mathrm{NL}}$), as shown in the last column in Fig. 4.

First, the color of the facial surface (first row in Fig. 3) is inherited by the symmetry profile, i.e., if a line segment in the symmetry profile is the intersection between the symmetry plane and a triangle in the facial mesh S, the color of that line segment is the same as the color of that triangle. In this way, we get a colored symmetry profile, as shown in Fig. 3.

We then use some prior knowledge to extract the three essential points $\boldsymbol{P}_{\mathrm{NT}}$, $\boldsymbol{P}_{\mathrm{NB}}$, and $\boldsymbol{P}_{\mathrm{NL}}$ on the symmetry profile. Suppose the symmetry profile is represented by a normal arc-length parameterized curve $C(s)$. The first essential point to be extracted is the nose tip $\boldsymbol{P}_{\mathrm{NT}}$. In the colored symmetry profile, the nose is a relatively long blue segment, and it is closer to the center point $C(0.5)$ of the symmetry profile than any other long blue segment (such as the chin). These characteristics distinguish the nose segment from the other geometric features in the symmetry profile. Suppose the blue nose segment is denoted as $[s_0^n, s_1^n]$. We take the point with the largest absolute curvature value κ in that segment as the nose tip $\boldsymbol{P}_{\mathrm{NT}}$, i.e.,

$$s_{\mathrm{NT}} = \arg\max_{s\in(s_0^n, s_1^n)}(|\kappa(s)|)\ . \tag{16}$$

If the curvature value at $\boldsymbol{P}_{\mathrm{NT}}$ is negative, the curvature value at each vertex on the profile is multiplied by -1.

The symmetry profile is divided into an upper (from $\boldsymbol{P}_{\mathrm{NT}}$ to the end of the forehead) and a lower (from $\boldsymbol{P}_{\mathrm{NT}}$ to the end of the chin) part by $\boldsymbol{P}_{\mathrm{NT}}$. If $\left|s_{\mathrm{NT}} - s_0^n\right| < \left|s_{\mathrm{NT}} - s_1^n\right|$, then the direction from s_{NT} to s_0^n is toward the chin; otherwise, the direction from s_{NT} to s_0^n is toward the forehead. In this way, we orient the profile vertically and distinguish the two parts.

Based on this orientation, the first point below $\boldsymbol{P}_{\mathrm{NT}}$ with local minimal curvature value κ is taken as $\boldsymbol{P}_{\mathrm{NT}}$. Above $\boldsymbol{P}_{\mathrm{NT}}$, the point with the smallest curvature value is taken to be $\boldsymbol{P}_{\mathrm{NB}}$. $\boldsymbol{P}_{\mathrm{NB}}$ is not necessarily the first point with local minimal curvature in the upper part of the face, as some people have extra local minimal curvature values on their noses (Fig. 4).

4 Similarity comparison

The three essential points $\boldsymbol{P}_{\mathrm{NT}}$, $\boldsymbol{P}_{\mathrm{NB}}$, $\boldsymbol{P}_{\mathrm{NL}}$ uniquely determine a coordinate system (Fig. 5). $\boldsymbol{P}_{\mathrm{NT}}$ is the origin; vector $\boldsymbol{V}_{\mathrm{TB}}$ represents the direction of the y axis, where $\boldsymbol{V}_{\mathrm{TB}} = (\boldsymbol{P}_{\mathrm{NB}} - \boldsymbol{P}_{\mathrm{NT}})/\left\|\boldsymbol{P}_{\mathrm{NB}} - \boldsymbol{P}_{\mathrm{NT}}\right\|$; the cross product of $\boldsymbol{V}_{\mathrm{TB}}$ and $\boldsymbol{V}_{\mathrm{TL}}$ coincides with the direction of the x axis, where $\boldsymbol{V}_{\mathrm{TB}} = (\boldsymbol{P}_{\mathrm{NL}} - \boldsymbol{P}_{\mathrm{NT}})/\left\|\boldsymbol{P}_{\mathrm{NL}} - \boldsymbol{P}_{\mathrm{NT}}\right\|$, and the z axis is determined by the right-hand rule. This coordinate system is called the Face Intrinsic Coordinate System (FICS).

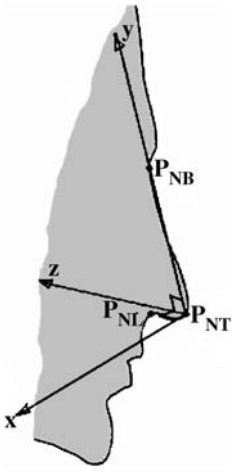

Fig. 5. Face Intrinsic Coordinate System (FICS). The y and z axes lie in the symmetry plane; the x axis is perpendicular to symmetry plane

Now, we have multiple choices for computing the similarity between the faces. A good choice should satisfy the following criteria:

(1) It should discriminate between individuals.
(2) It should be computationally efficient.
(3) It should concisely represent the face so as to reduce the size of the face database.

After various experiments, we determined that the mean distance between the aligned SFC representations of the faces was a good measure. By SFC representation we mean the three profiles on the facial surface, namely the symmetry profile, the forehead profile, and the cheek profile. The SFC representation is shown in Fig. 6. Define a plane $PL(\boldsymbol{P}_{\mathrm{NB}}, \boldsymbol{n})$, where $\boldsymbol{n} = \boldsymbol{P}_{\mathrm{NB}} - \boldsymbol{P}_{\mathrm{NT}}$ is the normal vector. The forehead profile and the cheek profile are obtained by intersecting the facial surface with two offset planes of $PL(\boldsymbol{P}_{\mathrm{NB}}, \boldsymbol{n})$, which are 3 cm arc length away from $PL(\boldsymbol{P}_{\mathrm{NB}}, \boldsymbol{n})$ in two opposite directions. The intersection point between the symmetry profile and the cheek profile is denoted as $\boldsymbol{P}_{\mathrm{c}}$, and that between the symmetry profile and the cheek profile is denoted as $\boldsymbol{P}_{\mathrm{f}}$. Selecting the forehead profile and the cheek profile avoids the eye regions that are not rigid enough. The SFC representation is relatively rigid in different expressions and effectively captures variation among individual faces. After the SFC representation is obtained, it is transformed to the FICS. Finally, the SFC representation rather than the space-consuming facial mesh is stored in the database.

The choice of 3 cm for determining the two transverse planes in the SFC representation is an empirical one. A slightly different distance could be used as long as the corresponding profiles in different scans of the same individual are at the same location. This is guaranteed by the following face comparison procedure (not directly by the 3 cm criterion). When a new face S^1 is to be compared with a face S^2 in the database (in SFC representation), we extract the three essential points of S^1 and convert the facial mesh into its FICS. The symmetry profiles of S^1 and S^2 are registered using the ICP algorithm again. Assuming the nose to be a fairly rigid feature, only the points between $\boldsymbol{P}_{\mathrm{NL}}$ and $\boldsymbol{P}_{\mathrm{NB}}$ on the two symmetry profiles respectively are used to optimize the alignment. Since the symmetry profiles are all in their FICSs, the initial relative position of the symmetry profiles guarantees the convergence of ICP. The computation expense in this procedure is almost negligible, for the number of points between $\boldsymbol{P}_{\mathrm{NL}}$ and $\boldsymbol{P}_{\mathrm{NB}}$ on the symmetry profiles is not large, and their initial relative locations are very close. After registering the two symmetry profiles, we obtain the cheek profile and forehead profile of S^1 by intersecting the two planes that contain the cheek profile and the forehead profile of S^2 with the mesh surface of S^1. Finally, a translation is performed to make $\boldsymbol{P}_{\mathrm{f}}^1$ and $\boldsymbol{P}_{\mathrm{f}}^2$ as well as $\boldsymbol{P}_{\mathrm{c}}^1$ and $\boldsymbol{P}_{\mathrm{c}}^2$ coincide (Fig. 6c).

After the SFC representations of two faces are registered, the similarity measure between them can be calculated. Let $L1$ and $L2$ be two profiles. Because the distance between two polylines is directional, i.e., the mean dis-

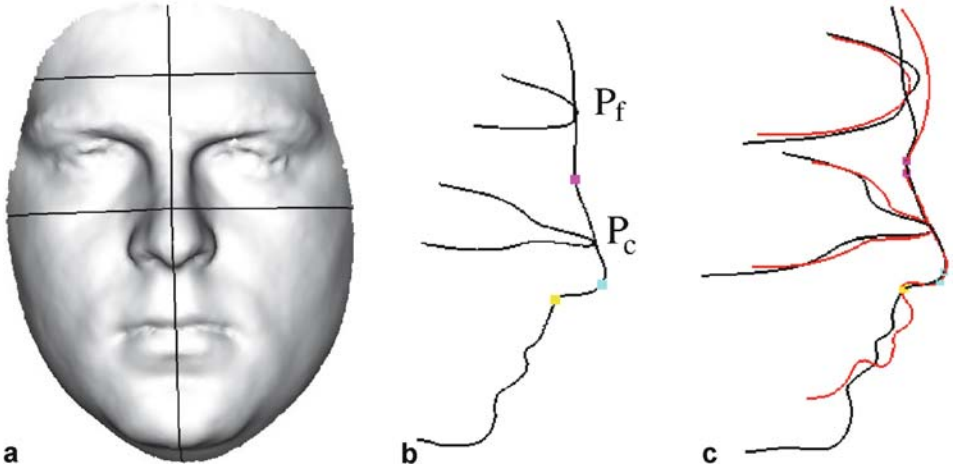

Fig. 6a–c. SFC representation. **a** Front view. **b** Isometric view. **c** Isometric view of two registered SFC representations (from different individuals)

Fig. 7. Distance from *black* profile to *red* one. Points on gray part are automatically discarded

tance from $L1$ to $L2$ and that from $L2$ to $L1$ might be different, we define

$$E_1 = \frac{1}{N_{L1}} \sum_{\boldsymbol{p}_1 \in L1} min_{\boldsymbol{p}_2 \in L2} d(\boldsymbol{p}_1, \boldsymbol{p}_2)\,, \tag{17}$$

$$E_2 = \frac{1}{N_{L2}} \sum_{\boldsymbol{p}_2 \in L2} min_{\boldsymbol{p}_1 \in L1} d(\boldsymbol{p}_2, \boldsymbol{p}_1)\,, \tag{18}$$

where N denotes the number of sampled points on the profile and d is the Euclidean distance. The similarity measure between the two profiles $L1$ and $L2$ is defined as

$$E = \tfrac{1}{2}(E_1 + E_2)\,. \tag{19}$$

It should be noted that the corresponding profiles of the two compared faces might be different in length. The longer parts of the profiles (gray segment in Fig. 7) are automatically truncated for similarity computation.

According to Eqs. 17–19, we compute three similarity measures E_S, E_F, and E_C, i.e., the mean distances between the symmetry profiles, the forehead profiles, and the cheek profiles, respectively. In Sect. 5, we show experimental results on face authentication and recognition using the three measures and their weighted combination defined as

$$E_W = w_S E_S + w_F E_F + w_C E_C\,, \tag{20}$$

where w represents the weight of a measure.

5 Experiments

5.1 Data acquisition

We use a stereo-image-based scanning system from 3Q Inc. (`http://www.3q.com`) in our experiments to scan the faces. The scanner uses four cameras to guarantee the coverage of the ear-to-ear region of a face, allowing large pose changes (the first row of Fig. 8 shows the frontal view of some scans, which illustrates the pose changes involved). It outputs textured 3D triangular meshes (about 20,000 vertices) in a natural-light environment. The facial meshes in the experiment of this paper were obtained using a semiautomatic preprocessing procedure to trim off the nonfacial regions in the raw mesh. This procedure can now be done fully automatically (see Sect. 5.4 for more discussion). In this paper, we discard the texture information and keep only the triangular mesh in our algorithm to explore the capability and potential of the geometry method. This is partly because the texture information is not reliable in some cases, for example when using makeup. Also, using only the triangular mesh makes the algorithm suitable for dealing with datasets obtained by other types of scanners that do not capture texture.

We scanned 166 individuals in our experiments, of which 32 individuals have multiple scans and the others has one scan. The tested individuals cover a wide ethnic and age diversity, different facial hair conditions, and var-

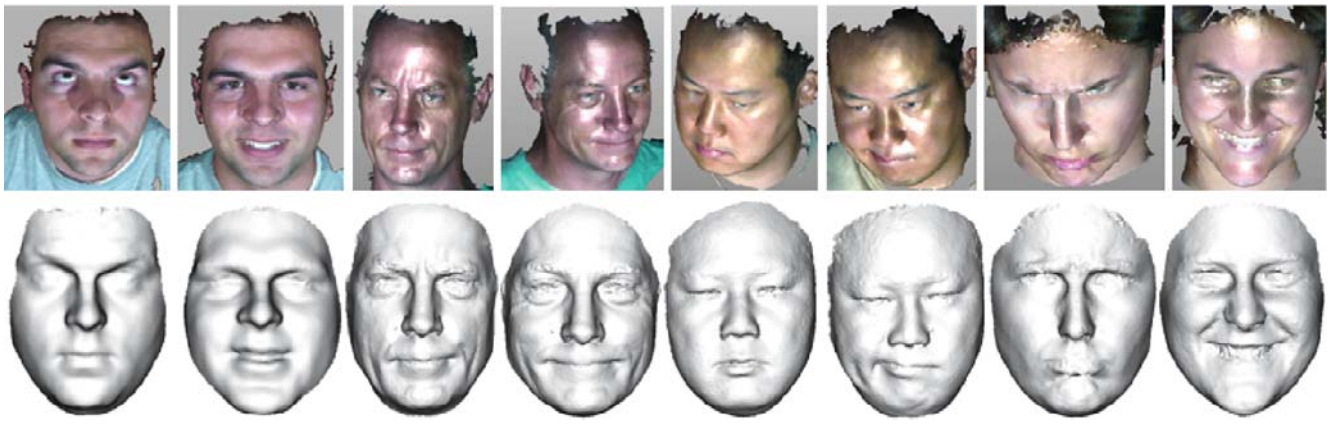

Fig. 8. Part of expressions for comparisons between scans from same individuals. *First row*: front view of textured 3D meshes output by scanner (images are chopped to highlight expressions). *Second row*: corresponding trimmed faces without texture

ious expressions. The time interval between some of the scans of the same person is more than 1 year. No one in our experiments wore glasses.

5.2 Authentication

Face authentication involves performing verification based on a one-to-one search to validate the identity claim of an individual (i.e., access control for a building, room, or for making a transaction at an ATM terminal). In the applications of face authentication, a similarity threshold should be determined for accepting or rejecting a claim.

The first face authentication experiment focused on testing the influence of expression. We first compared 300 randomly selected pairs of faces from different individuals (denoted as D-Comparison). To obtain the comparisons between same individuals, each pair of scans in different expressions of the 32 individuals who have multiple scans are compared. This generated 192 same-person comparisons (denoted as S-Comparison). Figure 8 illustrates part of the expressions in the S-Comparisons.

Here we give some statistical terminologies for face authentication. Given pairs of facial meshes of same individual, the false rejection rate (FRR) is the percentage of scans that is falsely rejected as belonging to different individuals. Given pairs of facial meshes of different individuals, the false acceptance rate (FAR) is the percentage of scans that is falsely accepted as belonging to the same individual. If FRR = FAR under a threshold of a specific measure, then that percentage is called the equal error rate (EER), which can be used to evaluate the performance of the comparison algorithm.

The weights in Eq. 20 are optimized using LDA (linear discriminant analysis). The optimization result in this experiment is $w_S = 0.20$, $w_F = 0.65$, $w_C = 0.15$. Figure 9 is the ROC curves of face authentication on scans with different expressions, which shows that the EER of the weighted combination measure E_W is 10.8%.

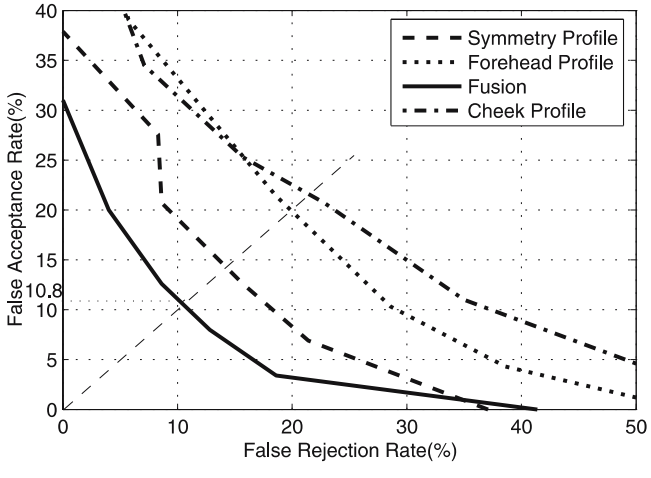

Fig. 9. ROC curves of authentication experiment on scans with different expressions

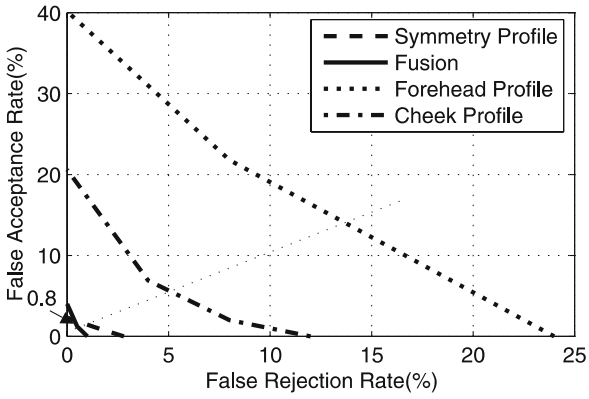

Fig. 10. ROC curves of authentication experiment on scans with normal expressions

In the second authentication experiment, the comparisons between the same individuals are conducted on scans with a normal expression. Figure 10 shows the EER of the measures, which demonstrates that the combined measure E_W outperforms the other measures with 0.8% EER.

5.3 Recognition

While the focus of this paper is on face authentication, the proposed method can be used in face recognition tasks as well. In face recognition applications, one-to-many searches are performed to identify an unknown individual based on comparison to a database of known individuals (e.g., law enforcement and surveillance). Unlike the authentication scenario, face recognition does not need a criterion to determine if two scans represent the same individual. Instead, face recognition needs to find the "best match" in terms of some similarity measure of a given scanned datum from the database.

We did face recognition experiments on 32 individuals. The database contains the facial meshes of 166 individuals, which include the 32 tested individuals. One different scan of each tested individual is compared to all 166 scans in the database. The performance of the similarity measures E_S, E_F, E_C, and E_W in face recognition is illustrated in Fig. 11. As in the authentication experiments, the weighted combination (E_W) is still the best measure in face recognition and has an 87.5% rank-one recognition rate when the tested individuals have different expressions in their two scans. When the tested individuals have a normal expression in their two scans, the rank-one recognition rate goes up to 96.9%.

5.4 Discussion

It takes an average of 2.8 s to obtain the SFC representation from a facial mesh. The average size of the SFC

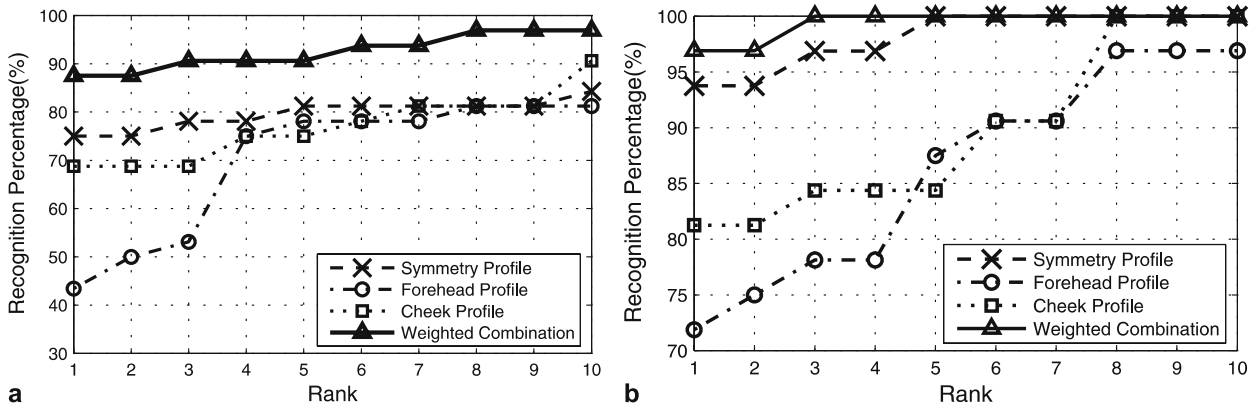

Fig. 11a,b. Performance results in face recognition experiment. **a** Results on scans in special expressions. **b** Results on scans in normal expression

representation is about 15 KB, which is 100 times smaller than the size of the triangular mesh representation. The most time-consuming stage is the ICP algorithm for aligning the original and the mirrored meshes, which takes an average of 1.2 s. The second time-consuming procedure is the mean curvature computation of the facial mesh, which takes 1.0 s. Comparison between two SFC representations takes an average of 0.5 s. The times reported in this paper are experimental results on a 1-GHz Pentium IV PC with 512 MB RAM.

The 10.8% EER and 87.5% rank-one recognition rate are among the best published 3D face recognition results for individuals with varied facial expressions. As expected, better results have been obtained for scans in normal facial expression. Our profile-based method clearly offers promise based on the experimental results and the relative rigidity of the chosen profiles.

As mentioned above, the facial meshes in the experiments of this paper are obtained by a preprocessing procedure to trim off the nonfacial parts. Our latest research has worked out a method to automatically clean up the raw meshes. The key ingredient of the cleaning method is to extract the face symmetry plane from the raw mesh by generalizing the basic idea of the MarkSkirt operator. Details on automatic face cleaning from the raw meshes will appear in a subsequent paper. Once the symmetry plane can be extracted from the raw meshes, the whole process from 3D image capture to face comparison and authentication is fully automatic. This automation is critical in practical authentication or recognition applications.

6 Conclusion and future work

We have demonstrated an approach for human face authentication and recognition based on 3D facial meshes. The method is based on the extraction of the bilateral symmetry plane and the recognition of three essential points of the face geometry, which prove to be robust to asymmetry boundaries and appearances of the scans. We also put forward a compact representation, namely the SFC representation, of the 3D face geometry. Face authentication and face recognition are studied by comparing the mean distance between SFC representations. The weighted combination E_W of the similarity measures of the symmetry profile, the forehead profile, and the cheek profile generates promising authentication and recognition rates under varied expressions. Authentication and recognition experiments also show that false results are mainly caused by extreme expressions. In normal expression, the EER and rank-one recognition rate are 0.8% and 96.9%, respectively. The time and space consumption in the proposed method is acceptable in typical face comparison scenarios.

Although we have obtained promising results using only 3D geometry information, there is room to explore the use of texture information as an additional clue in face comparison tasks. Other future work includes expanding the size of the database, managing the database in a more efficient way, and incorporating the generalized MarkSkirt operator in the authentication and recognition process to deal with the raw meshes directly.

Acknowledgement This work is supported by the National Science Foundation (NSF, Grant 0312849). Dr. Liyan Zhang was supported by the National Science Foundation of China (NSFC, Grant 50475041) and the Huo Ying-Dong Educational Foundation (Grant 03-91053).

References

1. Benz, M., Laboureux, X., Maier, T., Nkenke, E., Seeger, S., Neukam, F., Häusler, G.: The symmetry of faces. In: Proceedings of Vision, Modeling and Visualization, pp. 43–50 (2002)
2. Besl, P., McKay, N.: A method for registration of 3-D shapes. IEEE Trans. Pattern Anal. Mach. Intell. **14**(2), 239–256 (1992)
3. Beumier, C., Acheroy, M.: Automatic 3D face authentication. Image Vis. Comput. **18**(4), 315–321 (2000)
4. Beumier, C., Acheroy, M.: Automatic face verification from 3D and grey level clues. Pattern Recog. Lett. **22**(12), 1321–1329 (2001)
5. Blanz, V., Vetter, T.: Face recognition based on fitting a 3D morphable model. IEEE Trans. Pattern Anal. Mach. Intell. **25**(9), 1063–1074 (2003)
6. Bowyer, K., Chang, K., Flynn, P.: A survey of 3D and multi-modal 3D+2D face recognition. Notre Dame CSE Technical Report (2004)
7. Bronstein, A., Bronstein, M., Kimmel, R.: Expression invariant 3D face recognition. In: Proceedings of the International Conference on Audio and Video Based Biomeasure Person Authentication, pp. 62–70 (2003)
8. Cartoux, J., Lapreste, J., Richetin, M.: Face authentification or recognition by profile extraction from range images. In: IEEE Computer Society Workshop on Interpretation of 3D Scenes, pp. 194–199 (1989)
9. Chang, K., Bowyer, K., Flynn, P.: Face recognition using 2D and 3D facial data. In: Proceedings of the Workshop in Multimodal User Authentication, pp. 25–32 (2003)
10. Chua, C., Han, F., Ho, Y.: 3D human face recognition using point signature. In: Proceedings of the 4th IEEE International Conference on Automatic Face and Gesture Recognition, p. 233 (2000)
11. Hallinan, P., Gorden, G., Yuille, A., Giblin, P., Mumford, D.: Two and three-dimensional patterns of the face. Peters, Wellesley, MA (1999)
12. Hamann, B.: Curvature approximation for triangulated surfaces. In: Farin, G., Hagen, H., Notemeier, H., Knodel, W. (eds.) Geometric Modelling. Springer, Berlin Heidelberg New York, pp. 139–153 (1993)
13. Kazhdan, M., Chazelle, B., Dobkin, D., Funkhouser, T., Rusinkiewicz, S.: A reflective symmetry descriptor for 3D models. Algorithmica **38**(1), 201–225 (2003)
14. Lee, M., Ranganath, S.: Pose-invariant face recognition using a 3D deformable model. Pattern Recog. **36**(8), 1835–1846 (2003)
15. Liu, Y., Schmidt, K., Cohn, J., Weaver, R.: Facial asymmetry quantification for expression invariant human identification. Comput. Vis. Image Understand. **91**(1–2), 138–159 (2003)
16. Minovic, P., Ishikawa, S., Kato, K.: Three-dimensional symmetry measurement of medical entities. In: Proceedings of the 11th International Conference on Pattern Recognition: Conference A: Computer Vision and Applications, pp. 457–460 (1992)
17. Moreno, A., Sánchez, Á., Vélez, J., Díaz, F.: Face recognition using 3D surface-extracted descriptors. In: Proceedings of the 7th Irish Conference on Machine Vision and Image Processing, Antrim, N. Ireland (2003)
18. O'Mara, D., Owens, R.: Measuring bilateral symmetry in three dimensional magnetic resonance images. In: Attikiouzel, Y. (ed.) 1996 IEEE Region Ten Conference: Digital Signal Processing Applications, IEEE Service Center, pp. 151–156 (1996)
19. Reisfeld, D., Wolfson, H., Yeshurun, Y.: Detection of interest points using symmetry. In: Proceedings of the International Conference on Computer Vision, pp. 62–65 (1990)
20. Turk, M., Pentland, A.: Face recognition using eigenfaces. In: Proceedings of the Conference on Computer Vision and Pattern Recognition, pp. 586–591 (1991)
21. Tuzikov, A., Colliot, O., Bloch, I.: Brain symmetry plane computation in MR images using inertia axes and optimization. In: Proceedings of the International Conference on Pattern Recognition, pp. 516–519 (2002)
22. Wu, Y., Pan, G., Wu, Z.: Face authentication based on multiple profiles extracted from range data. In: Kittler, J., Nixon, M. (eds.) International Conference on Audio- and Video-Based Biometric Person Authentication. Lecture notes in computer science, vol 2688. Springer, Berlin Heidelberg New York, pp. 515–522 (2003)
23. Zhao, W., Chellappa, R., Rosenfeld, A.: Face recognition: a literature survey. ACM Comput. Surv. **35**(4), 399–458 (2003)

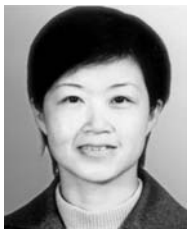




DR. LIYAN ZHANG is a professor at the CAD/CAM Research Center, Nanjing University of Aeronautics and Astronautic, P.R. China. Her research interests include geometric modeling, image-based 3D reconstruction, and reverse engineering in product design. She was recently supported by the Program for New Century Excellent Talents in China.

DR. ANSHUMAN RAZDAN is the director of PRISM: Partnership for Research In Spatial Modeling and affiliate assistant professor in the Department of Computer Science and Engineering at Arizona State University, Tempe, AZ. His research interests include computer-aided geometric design and computer graphics, NURBS curves and surface approximation, compression of 3D data, and use of high-bandwidth networking for scientific visualization and feature segmentation. He is a PI on several NSF grants including a recent ITR grant for 3D face authentication for homeland security. He has a B.S. and M.S. in mechanical engineering and Ph.D. in computer science. He recently founded a new 3D immersive visualization facility at ASU called The Decision Theatre (DT) and also serves as its director of research and technology. Additional information is available at `http://prism.asu.edu` and `http://dt.asu.edu`.

GERALD FARIN received his Ph.D. in mathematics from the Universtiy of Braunschweig, Germany in 1979. He is the author of *Curves and Surfaces for CAGD* (5th edn.), *NURBS* (2nd edn.), *Practcal Linear Algebra*, and *The Essentials of CAGD*. He is editor-in-chief of the journal Computer-Aided Geometric Design. His industrial experience consists of 4 years of CAD/CAM development at Mercedes-Benz, Stuttgart, Germany. He subsequently worked at the University of Utah (Mathematics) and Arizona State University (Computer Science).

JOHN C. FEMIANI received his B.S. in studio art with an emphasis on 3D modeling from Arizona State University, Tempe, AZ, USA in 2000. Since 2002 he has been a Ph.D. student at the Arizona State University Department of Computer Science in the Fulton School of Engineering. He has worked as a research assistant in the Partnership for Research in Spatial Modeling (PRISM), where he has pursued research in algorithms and techniques for 3D modeling as well as 3D pattern matching and recognition.

MYUNGSOO BAE is currently enrolled in the Ph.D. program in the Department of Computer Science and Engineering at Arizona State University in Tempe, AZ and is a graduate research assistant at PRISM. His research interests lie broadly in the area of CAGD. These include surface matching and metrics for meshes, feature segmentation, and surface approximation using NURBS. He holds an M.S. in computer science from Arizona State University.

CHARLES LOCKWOOD is a lecturer in the Department of Anthropology at University College London. He received a B.Sc. from Duke University in 1992 and Ph.D. from the University of the Witwatersrand (Johannesburg, South Africa) in 1997. He held a postdoctoral position and was then assistant professor at the Institute of Human Origins at Arizona State University from 1997 to 2003, when this research began. Lockwood's research centers on the application of morphometric techniques to the evolution of the human skull, addressing questions of intra- and interspecific variation and how patterns of variation relate to the evolution of sex differences in skull shape. He serves on the editorial board of the Journal of Human Evolution.